Photofragmentation of OClO Clusters in a Supersonic Jet at 360 and 275 nm

Kathrin Fenner, Alan Furlan, and J. Robert Huber*

Physikalisch-Chemisches Institut, der Universität Zürich, Winterthurerstrasse 190, 8057 Zürich, Switzerland

Received: March 21, 1997; In Final Form: May 28, 1997[⊗]

Using photofragment translational energy spectroscopy, we studied the photochemical decay of chlorine dioxide (OClO) clusters in a cold beam with Ne as carrier gas. The products ClO, OClO, Cl_2O_3, and Cl_2O_4 generated by 360 nm excitation were—except for the fast ClO fragments which arise from monomer photodissociation—found to be slow moving and with broad time-of-flight distributions. They show an approximately thermal translational energy distribution of 300−500 K and a recoil anisotropy $\beta \approx 0$, as measured for the representative OClO product. Furthermore with excitation at 275 nm where the OClO monomer has no absorption, the same slow moving product species were created, indicating that they are evaporation products of excited cluster species. A reaction scheme is proposed which includes unimolecular photochemical decays and bimolecular cage reactions of initially formed fragments among themselves and with cluster constituents.

1. Introduction

The photochemistry of chlorine dioxide, OClO, has been studied in the gas phase, liquid solution, and cryogenic matrix. The complex photochemistry of this molecule, which is of interest due to its possible role in stratospheric ozone loss,[1−5] was found to depend strongly on the medium. Isolated molecules in the gas phase exhibit two reaction pathways. Following excitation into the $\tilde{A}^2A_2$ state, the predominant dissociation channel of OClO between 290 and 475 nm is the decay to $ClO(\tilde{X}^2\Pi) + O(^3P)$.[6−13] The analysis of the highly structured absorption spectrum in the near-UV region has indicated that the process is predissociative with the bending mode ν_2 and at higher energy also the asymmetric stretching mode ν_3, acting as promoting modes.[10,14−17] The second decay channel, yielding $Cl(^2P) + O_2(^3\Sigma_g^-, {}^1\Delta_g)$, was shown to be of minor importance; it has a maximum yield of 3.9 ± 0.8% at $\lambda_{exc} = 404$ nm which decreases to <0.2% at $\lambda_{exc} < 370$ nm.[6]

The suggestion that the presence of atmospheric aerosols (polar stratospheric clouds) may influence the photochemistry of OClO and ultimately lead to ozone loss,[4] has triggered the study of the photoinduced reaction of OClO embedded in solid and liquid matrices, as well as small gas-phase aggregates. In noble gas and amorphous ice matrices,[18−21] the formation of the chlorine peroxy radical ClOO, created by the photoisomerization or by cage recombination of the primary products ClO + O, has been observed. Using Fourier transform infrared (FTIR) spectroscopy after photolysis, Pursell et al.[22] reported a quantum yield of unity for the formation of ClOO from OClO in an ice matrix at 80 K. In the gas phase, however, this photoisomerization is not important.[6−8]

Simon and co-workers studied the photochemistry of OClO in liquid water[23] and sulfuric acid[24] solutions by picosecond time-resolved spectroscopy. In water, 90% of the excited molecules fragment into ClO + O and the remaining 10% form Cl + O_2. Since ∼5% of the generated O_2 is formed in the excited electronic state $^1\Delta_g$ and the rest in the ground state $^3\Sigma_g^-$, it was suggested that ClOO is responsible for most of the Cl production in the liquid phase because the excited states of ClOO electronically correlate to $O_2(^3\Sigma_g^-)$.

Apart from studies with highly diluted OClO in solid matrices, pure OClO films and aggregates were also investigated using temperature-programmed desorption, reflection infrared absorption and time-of-flight (TOF) spectroscopy. In a thin OClO film irradiated at 360 nm, Grassian and co-workers[25] identified OClO, ClO, and O_2 as the major photoproducts ejected into the gas phase, whereas Cl_2O_2 and Cl_2O_3 appeared to be the predominant products retained in the film.

Flesch et al.[26] studied the photofragmentation of chlorine dioxide aggregates $(OClO)_n$ in the range 349−373 nm by employing vacuum UV ionization followed by TOF mass analysis. They detected the products O_2, Cl_2O_3, Cl_3O_5, and OClO evaporated from excited aggregates. The structure of the product Cl_2O_3 and of the dimer Cl_2O_4 were explored by ab initio calculations.

In the present work photofragment translational energy spectroscopy (PTS)[27−30] is applied to study OClO clusters in a cold molecular beam. The photoproducts formed by photolysis at 360 and 275 nm are identified and the expansion conditions for cluster formation are characterized. The recoil anisotropies, β, are determined, and the kinetic energy distributions of the fragments are evaluated from the time-of-flight measurements.

2. Experimental Section

The experiments were carried out with a photofragment translational energy spectrometer described elsewhere.[31] It consists of a rotatable, pulsed molecular beam source, a 34.5 cm long drift tube, and a quadrupole mass spectrometer for mass filtering and detection. The photolysis laser beam crossed the molecular beam 65 mm from the piezoelectric pulsed nozzle. Laser pulses of 0.5−5 mJ ($\Delta\tilde{\nu} = 0.15$ cm^{-1}, $\tau \sim 6$ ns) were obtained by frequency-doubling the output of a Nd:YAG-pumped dye laser (Scanmate 2E).

OClO was generated by passing Cl_2 over $NaClO_2$. The $NaClO_2$ contained 2 mbar of H_2O to catalyze the reaction.[32] After completion of the reaction, the yellow product was passed through an additional U-tube filled with $NaClO_2$ and glassbeads and cooled with ice water to remove H_2O. Because OClO decomposes upon contact with metal, we used a metal-free inlet system and a specially designed Teflon molecular beam valve.[33] It should be noted that OClO is explosive at concentrations in excess of 10% atmospheric pressure.[32] For each measurement ∼50 mbar of fresh OClO was produced and transferred to a

* Corresponding author. Tel: +41/1-635 4461. Fax: +41/1-362 0139. E-mail jrhuber@pci.unizh.ch.

⊗ Abstract published in *Advance ACS Abstracts,* July 15, 1997.

S1089-5639(97)01028-1 CCC: $14.00

container that was then filled with Ne to a total pressure of 200−1500 mbar and automatically held at constant pressure. The velocity distribution of the molecular beam pulse $f(v) \sim v^2 \exp[-(v - v_s)^2/\alpha^2]$ was determined before and after each measurement, using a chopper wheel synchronized with the pulsed valve. The delay time between the nozzle opening and the chopper slit passing through the molecular beam was optimized for maximum dimer signal. The stream velocity v_s for this part of the molecular beam was measured to be 750 ± 40 m/s. The width of the distribution $\alpha = (2kT/m)^{1/2}$ was found to depend strongly on the total pressure and concentration of the OClO/Ne mixture. It ranged from 31 ± 3 m/s for 5% OClO in 1500 mbar of Ne to 52 ± 2 m/s for 5% OClO in 300 mbar of Ne, corresponding to OClO translational temperatures of 4 and 11 K, respectively. A time offset of 3.9 μs $(e/m)^{1/2}$ has been subtracted in all of the TOF spectra shown in order to correct for the transit time of the ions through the mass filter.[31]

The recoil anisotropies, parameter β, were determined by measuring the TOF intensity at different polarization angles, ϵ (angle between the electric field vector and the detector axis), and fitted according to the procedure described elsewhere.[34,35]

3. Results

The molecular beam pulse was analyzed at various mass filter settings by directing it via a chopper wheel directly into the mass spectrometer. The slotted wheel improved the selectivity in that only the central part of the molecular pulse could be selected and, moreover, protected the detector from being overloaded. The measurements were usually carried out at a backing pressure of $p_0 = 1050$ mbar and a 5% mixture of OClO in neon. The electron acceleration voltage of the ionizer was varied between 60 and 130 V in order to have a certain control over the fragmentation of the species of interest. Besides the parent molecule OClO ($m/e = 67$), we detected the dimer and the trimer ($m/e = 201$), as well as species at $m/e = 67 + 20n$ with $n = 1-7$ corresponding to $(OClO)(Ne)_n$ clusters. The abundance of the $n = 4-7$ clusters appeared to be greater than that for the $n = 1-3$ ones. Though not detected with our electron impact analyzer, it seems likely that also $(OClO)_m(Ne)_n$ clusters with $m > 1$ are formed under the present conditions. It is noted that the beam was free of other chlorine-containing species such as Cl_2O_3. A very weak signal was detected at $m/e = 32$ which increased slightly in time. The ratio of the integrated intensities $I(m/e = 32)/I(m/e = 67)$ reached a value of 0.07 after 2 h. We attribute the $m/e = 32$ signal to a spurious amount of O_2 in the inlet system rather than to cracking of OClO in the ionizer. This will have only a minor influence on the O_2 signal from cluster photolysis discussed in the next sections.

Following excitation at 360 nm and under backing pressure conditions $p_0 = 1050$ mbar for which OClO in Ne is subject to cluster formation, the bimodal photofragment TOF spectrum of ClO^+ shown in Figure 1a is obtained. The fast component with a maximum signal at ∼230 μs is reminiscent of the single ClO^+ peak signal measured previously from the monomer dissociation OClO → ClO + O using He as a carrier gas (cf. Figure 1a in ref 8). The slower and broader component is expected to be due to cluster formation. This assumption is supported by the TOF spectrum taken at $\theta = 9°$ of the parent molecule ($OClO^+$) emerging from clusters after laser excitation shown in Figure 1b. (It is noted that the spectra in Figure 1 represent difference spectra obtained by subtracting the signal without laser pulse excitation from that with laser excitation.) The excellent agreement between the slow component signal in Figure 1a and the $OClO^+$ spectrum in Figure 1b (see below)

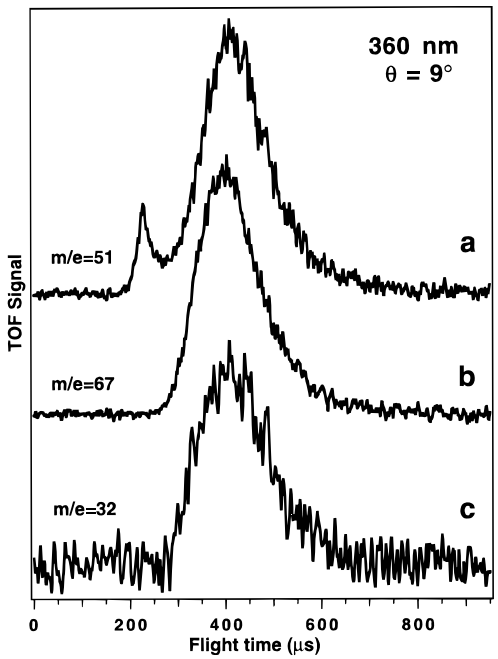

Figure 1. TOF distributions of species generated by photolysis of OClO monomers and aggregates at (a) $m/e = 51$ (ClO^+), (b) $m/e = 67$ ($OClO^+$), and (c) $m/e = 32$ (O_2^+). The spectra were recorded under a scattering angle $\theta = 9°$ and an excitation wavelength of 360 nm. The peak around 250 μs in spectrum a corresponds to ClO fragments from OClO monomers in the beam, whereas the broad peak at longer flight times is due to OClO molecules evaporated from clusters. The signal in spectrum c is attributed to O_2 fragments. Apart from the peak at 250 μs in spectrum a, all signals appear only under clustering conditions (5% OClO in Ne at 1050 mbar).

leads us to surmise that the ClO^+ peak in the former originates from OClO which is partially fragmented by electron impact in the detector. Since the degree of fragmentation of OClO to ClO (∼0.4), which was independently measured for the applied electron impact energy, also agrees well with the intensity ratio of the two signals in parts a and b of Figure 1 (∼0.4), we conclude that the slow ClO^+ peak in Figure 1a arises from OClO ejected from clusters upon photolysis.

The total center-of-mass translational energy distribution $P(E_T)$ of the recoiling photofragment pairs in the reaction is obtained by transforming an initially estimated $P(E_T)$ into a laboratory TOF distribution and refining it until a satisfactory fit to the recorded TOF data is achieved.[36] This forward convolution procedure requires knowledge of the masses of both photofragments. For the fast peak in the TOF spectrum (Figures 1a and 2a), which is due to the ClO + O pair, this requirement is satisfied, and a fit was easily achieved with the $P(E_T)$ given in Figure 2b showing an average translational energy $\langle E_T \rangle$ of 55−60 kJ/mol. The corresponding TOF spectrum in Figure 2a ($m/e = 51$, solid line) reproduces the fast peak at $t_{TOF} \sim 230$ μs. For the slow peak, however, the counterfragment of the OClO fragment is not known. Since it is anticipated that OClO is liberated from a dimer or a larger cluster, we carried out the fitting procedure[36] assuming two counterfragment masses of $m = 67$ and $m = 10^3$ and obtained the $P(E_T)$'s shown in Figure 2b. Each one of these distributions fits both TOF spectra, the one at $m/e = 51$ as well as that at $m/e = 67$, confirming that at both mass settings OClO fragments are detected. There is, however, a small part of the $m/e = 51$ spectrum, around $t_{TOF} = 270$ μs (Figure 2a), which lies outside the fit of the fast and the slow peak. This contribution is surmised to be due to ClO fragments having a smaller E_T than those giving rise to the fast peak (see Discussion).

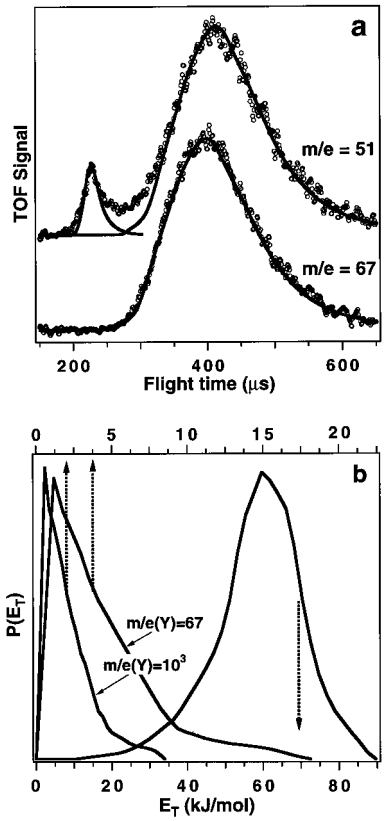

Figure 2. (a) TOF distributions measured at $m/e = 51$ and 67. The solid lines in panel a were obtained from the best fit of a forward convolution of the translational energy distributions $P(E_T)$ shown in panel b. The $P(E_T)$ peaking around 60 kJ/mol was calculated for a decay of the OClO monomer to ClO + O, whereas for the distributions peaking at 2−4 kJ/mol, a cluster fragmentation $(OClO)_n \rightarrow (OClO)_{n-1}$ + OClO was assumed, with $n = 2$ ($m/e = 67$) and $n = 25$ ($m/e \sim 1000$), respectively.

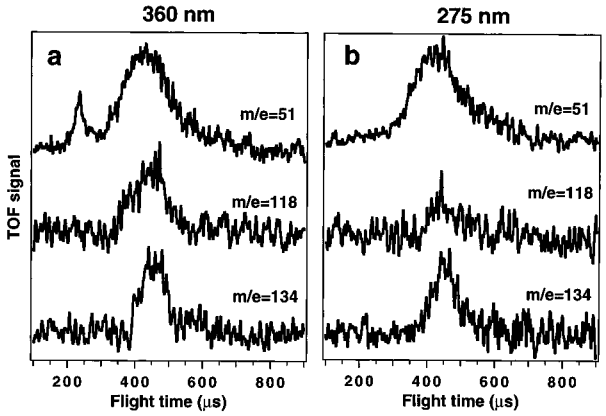

Figure 3. TOF distributions of the fragments ClO^+ ($m/e = 51$, except for the fast peak mainly from detector-fragmented OClO), $Cl_2O_3^+$ ($m/e = 118$), and $Cl_2O_4^+$ ($m/e = 134$) after photodissociation at 360 and 275 nm. At 275 nm, OClO molecules do not absorb, and hence the fast fragment peak measured at $m/e = 51$ (ClO^+) is not present.

Figure 1c displays the photofragment signal detected with the mass filter set at $m/e = 32$ which corresponds to O_2. The flight time of this species lies between 300 and 600 μs and is thus close to that of OClO given in spectrum Figure 1a,b but with a much weaker signal intensity. Furthermore, at $m/e = 118$ and 134 the TOF spectra of Figure 3a were observed which are due to Cl_2O_3 and Cl_2O_4, respectively. The species, having a flight time between 400 and 600 μs, are clearly not fragments from the OClO monomer photodissociation but must stem from dimers or higher cluster species.

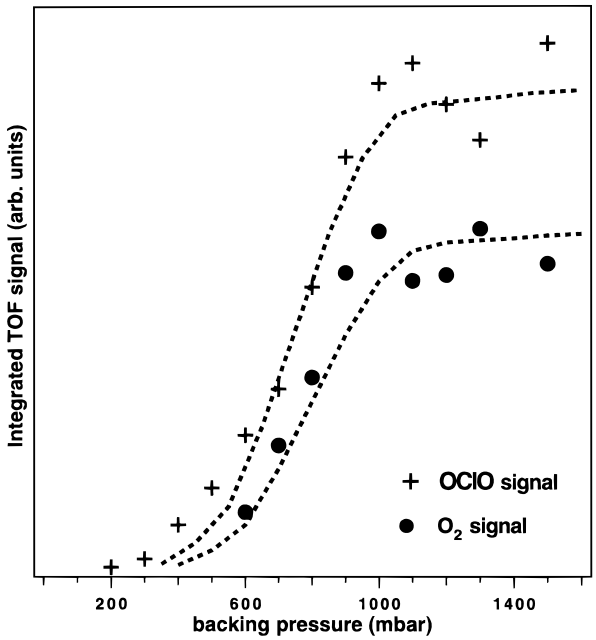

Figure 4. Pressure dependence of the TOF signal integrated over the slow peak at $m/e = 51$ (OClO detected as ClO^+, see Figure 1a) and the peak at $m/e = 32$ (O_2^+, see Figure 1c), measured with a 5% OClO/Ne mixture and following excitation at 360 nm.

The recoil anisotropy of the photofragments observed at $m/e = 51$ (Figure 1a) was obtained from the polarization dependence of the TOF signal measured with the linearly polarized photolysis laser.[34,35] At $p_0 = 300$, 600, and 900 mbar where no cluster, only a small amount of clusters, or a high cluster concentration is created, respectively, we determined the anisotropy parameter β for the fast fragments with $t_{TOF} = 220-310$ μs and for the slow ones with $t_{TOF} = 400-500$ μs as shown in Figure 1a. For the fast products β (300 mbar) $= 0.4 \pm 0.1$, β (600 mbar) $= 0.5 \pm 0.1$, and β (900 mbar) $= 0.4 \pm 0.1$, while for the slow fragments β is close to 0 irrespective of p_0.

The backing pressure dependence of the cluster formation[37,38] under the present experimental conditions was explored by measuring the integrated signal for the slow fragments in Figure 1a ($m/e = 51$; $t_{TOF} = 300-600$ μs) at various p_0. The signal arises from OClO photofragments which are generated from dimers and higher aggregates of OClO (see Discussion), and their production yield is therefore a direct measure of cluster formation. For a constant initial OClO concentration of 4% in Ne, the result is shown in Figure 4 indicating that the cluster formation starts at $p_0 \sim 300$ mbar and reaches a maximum at around 1200 mbar ("phase transition" curve[37,38]). In a similar manner the TOF signal of Figure 1c was analyzed to explore the p_0 dependence of the O_2 formation. The approximately parallel behavior of the two curves suggests the O_2 product to be closely related to the cluster formation. Complementary to these experiments we changed the OClO concentration in Ne between 0.5 and 4%, kept p_0 constant at 1000 mbar, and followed the Cl_2O_3 formation as observed by the TOF signal at $m/e = 118$ in Figure 2a. The Cl_2O_3 production was found to increase about linearly with the OClO source concentration supporting our assumption that also the Cl_2O_3 production depends on the cluster formation.

The absorption spectrum of OClO has been studied in considerable detail,[14−16] and also important features of the gas phase absorption of Cl_2O_2, Cl_2O_3, Cl_2O_6, and $ClOClO_3$ (chlorine perchlorate) have been reported.[39−41] Not surprisingly, the absorption spectrum of OClO, its dimer (not to be confused with chlorine perchlorate), and its higher aggregates produced

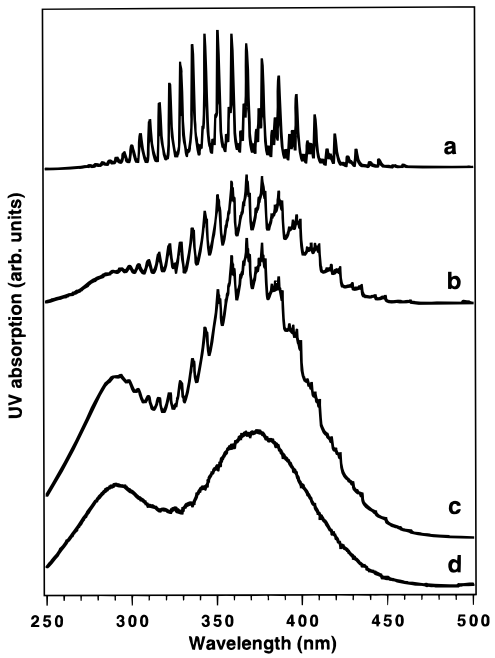

Figure 5. Absorption spectrum of OClO (a) in the gas phase (300 K, 0.6 mbar), (b) and (c) in a solid argon matrix at 15 K with [Ar]/[OClO] = 10 000 and 1000, respectively, and (d) difference of two matrix spectra taken with a dilution of [Ar]/[OClO] = 1000 and [Ar]/[OClO] = 10000.

in a jet expansion with a noble gas as carrier are not known. Since the absorption spectrum in a noble gas matrix at low temperature has some similarities with such a spectrum, we carried out Ar matrix absorption measurements using various OClO:Ar mixtures. Figure 5 exhibits the low-energy part of the OClO absorption spectrum between 250 and 500 nm in (a) the gas phase and (b), (c), and (d) in a solid Ar matrix at ~15 K. With increasing OClO concentration the matrix spectrum exhibits an additional band with a maximum around 290 nm and a growing background associated with the $\tilde{A}^2A_2 \leftarrow \tilde{X}^2B_1$ absorption of OClO at ~360 nm. A difference spectrum of (b) and (c) results in spectrum (d) which has two distinct maxima. Since the IR spectrum of these matrix samples shows no absorption due to species such as Cl_2O_3[21] or $ClOClO_3$,[42] we tentatively assign the absorption to a dimer and possibly higher aggregates of OClO. With this in mind we tuned the excitation laser to 275 nm and measured the TOF spectra for $m/e = 51$, 118, and 134 shown in Figure 3b. Since at 275 nm the monomer has no absorption, which is consistent with the absence of the fast peak in the TOF spectrum compared with the corresponding one in Figure 3a, the photofragments Cl_2O_3 and Cl_2O_4 as well as the slow OClO are indicated to originate from a species different from the monomer, very probably from an OClO cluster.

4. Discussion

Decay of the Monomer and Clusters at 360 nm Excitation. The molecular beam generated in our experiments contained the monomer OClO, the dimer $(OClO)_2$, the trimer $(OClO)_3$, the clusters $(OClO)Ne_m$, and probably also the aggregates $(OClO)_nNe_m$ with $n, m > 1$. On crossing this beam with a laser pulse at 360 nm (corresponding to 331 kJ/mol), the products ClO, O_2, Cl_2O_3, and Cl_2O_4 as well as OClO were detected. These products agree with the findings of Flesch et al.[26] who studied the photodissociation of OClO and its aggregates produced by expansion in He at $p_0 = 3.5$ bar. On the basis of our measured translational energy distribution and the anisotropy parameter β, the fast ClO fragments can unambiguously be assigned as emerging from the monomer dissociation

$$OClO \xrightarrow{h\nu} ClO^\bullet + O^\bullet \qquad (1)$$

which involves a dissociation energy $D_0 = 245$ kJ/mol[7,8] and an available energy $E_{avl} = h\nu - D_0 = 86$ kJ/mol for the fragments, assuming a negligible internal energy of the jet-cooled parent molecule.

The translational energy distribution of ClO + O shown in Figure 2b is in excellent agreement with that found in previous experiments on the monomer photodissociation.[8] That analysis showed the $ClO(\tilde{X}^2\Pi)$ fragment to be produced in the vibrational states $\nu = 1-6$ with $\langle E_T \rangle = 55$ kJ/mol and O in the ^3P state.[8] Also the recoil anisotropy observed for the fast ClO peak is very similar to the value determined previously.[8] The slightly increased β value in the present work, $\langle\beta\rangle = 0.45 \pm 0.1$, relative to $\beta = 0.36 \pm 0.05$ is attributed to the colder beam, due to the use of Ne instead of He as the carrier gas.[43] This reduces the rotational temperature of the parent molecule from $T_{rot} \approx 40$ K to ≈ 10 K. In both cases the upper limit dissociation lifetime deduced from the β parameter[44,45] is <2−5 ps.

The photodissociation of OClO in a cluster environment at 360 nm, which is close to the absorption maximum of the monomer, is expected to proceed according to the reactions

$$\{OClO\} \xrightarrow{h\nu} ClO^\bullet + O^\bullet \qquad (2a)$$

$$\xrightarrow{h\nu} ClOO \rightarrow Cl + O_2 \qquad (2b)$$

where the braces indicate the molecule being a part of a cluster. On the basis of the results of previous cluster studies on other systems,[37,38] reaction 2a will create ClO fragments with a reduced E_T compared to the free monomer (eq 1). Indeed the TOF spectrum at $m/e = 51$ (Figures 1a and 2a) exhibits a contribution at $t_{TOF} \sim 270\ \mu$s which could not be fit by the two $P(E_T)$ distributions of Figure 2b and which was surmised to stem from slower ClO fragments compared to those responsible for the fast peak. Reaction 2a might therefore be the source of this spectral feature. This reaction is expected to be in competition with the isomerization 2b. While this rearrangement is rather inefficient in an isolated monomer at 360 nm irradiation,[6,7] it has been proposed to occur in cold matrices.[18−21] The cluster environment prevailing under our expansion conditions could therefore promote this process. Since the isomer ClOO has a Cl−O bond dissociation energy of only ~20 kJ/mol,[46] the internal energy of ClOO acquired through the 360 nm photoisomerization will probably be sufficient to induce the decay to $Cl + O_2$. Indeed, oxygen molecules have been detected (Figure 1c) but—consistent with previous results—only if the cluster formation is substantial as demonstrated in Figure 4 where the O_2 TOF signal intensity follows the cluster formation process.

Flesch et al.[26] have suggested the "product" OClO to arise from evaporation of excited aggregates. Due to fragmentation in the ionizer we observed this species at $m/e = 51$, but also at $m/e = 67$ using a scattering angle $\theta = 9°$. The translational energy distribution $P(E_T)$ of OClO given in Figure 2 peaks at 1−2 kJ/mol and has a high-energy tail up to 8−16 kJ/mol depending on the choice of the unknown counterfragment. This $P(E_T)$ can be roughly described by a Boltzmann distribution with $T = 300-500$ K and thus supports the notion that the excited cluster constituent, most likely OClO or $(OClO)_2$, transfers its excess photon energy to the cage which is heated up and evaporates, ejecting OClO and Cl_2O_4. In addition to

reaction 2, these findings lead us to propose the decay of the dimer or caged dimer according to

$$\{(OClO)_2\} \xrightarrow{h\nu} OClO + OClO \quad (3a)$$

$$\xrightarrow{h\nu} O + ClOOClO \rightarrow O + OCl + OClO \quad (3b)$$

$$\xrightarrow{h\nu} Cl_2O_2 + O_2 \quad (3c)$$

This reaction scheme is also representative for reactions $(OClO)_n \rightarrow (OClO)_{n-1} + OClO$ etc. with $n > 2$ or $(OClO)Ne_m \rightarrow OClO + mNe$ but we confine our discussion to the dimer case. The structure of the dimer, although investigated in a crystal,[47] is not yet established in the gas phase or in a cluster, but results of ab initio calculations favor the following three structures:

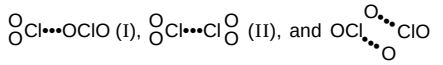

While Flesch et al.[26] prefer structure I, which has a bond dissociation energy of ~22 kJ/mol, we found structure III, consistent with the crystal structure, to be most favorable. Since a decision between I and III seems not yet to be possible, we merely assume in the following discussion that the dimer has a bond dissociation energy of ~20 kJ/mol. Photoexcitation of this cluster constituent at 360 nm is considered to include as a primary process the dissociation of the dimer into two OClO fragments (eq 3a) and/or the Cl−O bond scission (eq 3b) in analogy to the monomer decay eq 2a. With respect to the dissociation energy, ~20 kJ/mol for the dimer and 245 kJ/mol for the Cl−O bond rupture, it would appear that reaction 3a is faster than reaction 3b. If this is true, the two OClO fragments share an available energy exceeding 300 kJ/mol which, at least in part, is transferred to the cage, evaporating the latter and yielding approximately thermalized OClO species. Such fragments were detected in our TOF measurements (Figure 1b). It is also conceivable—though with a low probability—that the energy partitioning among the two OClO moieties is such that one of the fragments receives an internal energy greater than 245 kJ/mol of E_{avl} and may therefore decay in a second step to O + ClO. An uncaged ClO could then be detected having a smaller kinetic energy compared to the corresponding one from the monomer reaction 1. However, to attribute the small contribution of slow ClO fragments indicated in the TOF spectrum ($t_{TOF} \sim 270$ μs) of Figure 2 to the product of this secondary decay might appear speculative in view of the extreme energy partitioning required in the first step for the second step to occur.

Reaction 3b produces O and Cl_2O_3, the latter of which has been found in our TOF measurements. We can, however, not exclude that the internal energy distribution in the Cl_2O_3 product may be such that a part of these molecules decays further to ClO + OClO. The structure of Cl_2O_3 emerging from the dimer dissociation is not known. Ab initio calculations[26] predict the energetically most favorable structure to be $ClO-Cl\overset{O}{\underset{O}{}}$. This species is produced not only in the photodissociation of OClO clusters but also in solution[23,24] or in the photolysis of thin OClO films.[25] Finally, reaction 3c appears to be inefficient. This type of a concerted reaction involves a rather unfavorable transition state and is therefore considered not to be competitive with the direct decay reactions 3a and step 1 of 3b. Furthermore at the mass setting corresponding to Cl_2O_2 definitively no signal was detected.

Bimolecular Cage Reactions. The two fragments O and ClO generated in reaction 2a, and possibly in 3b if Cl_2O_3 is subject to a further decay, are highly reactive. They can be temporarily trapped by the cage to react with a cage-forming species, and the products may subsequently escape from the evaporating cluster to become amenable to TOF detection. The results in cold inert noble gas matrices[18−21] suggest also the possibility of a recombination of O and ClO to the isomer ClOO.

$$\{ClO + O\} \rightarrow ClOO \rightarrow Cl + O_2 \quad (4)$$

In a subsequent step ClOO may decay to Cl and O_2 depending on the internal energy of the isomer as discussed for reaction 2b. The reaction of the initially prepared hot ClO and O fragments with an OClO cluster constituent are expected to proceed to the final product species Cl_2O_3 and O_2 which both have been observed in the TOF measurements.

$$\{ClO + OClO\} \rightarrow Cl_2O_3 \quad (5)$$

$$\{O + OClO\} \rightarrow O_2 + ClO \quad (6)$$

Both reactions are exothermic with $\Delta H = -46.4$ kJ/mol[48] for reaction 5 and $\Delta H = -242$ or -147 kJ/mol[49] for reaction 6 depending whether O_2 is produced in the $^1\Delta_g$ or $^3\Sigma_g^-$ state, respectively. A substantial heating of the cluster environment is therefore expected.

The proposed reaction scheme 1−6 accommodates the present and previous data,[8,26] in particular the observed species ClO, OClO, Cl_2O_3, and O_2. The dimer Cl_2O_4, not especially discussed above, is considered to be an evaporation product from the excited aggregate.

Products at 275 nm Excitation. Since the additional absorption around 290 nm in the matrix environment (Figure 5d) may also exist in a cluster beam, we repeated the photodissociation experiment at 275 nm. At this wavelength, where the OClO molecule does not absorb, we detected the same fragments OClO, Cl_2O_3, and Cl_2O_4 as with the 360 nm excitation except of course the fast ClO fragments from the monomer dissociation. (Due to the low *S*/*N* ratio an unambiguous detection of the expected O_2 could not be obtained.) All these products must therefore be associated with cluster species of OClO as considered with the proposed reactions 2−6. Thus, the additional absorption revealed in the matrix spectrum of Figure 5 allows us to directly excite dimers, trimers, and maybe even higher aggregates of OClO when $\lambda < 290$ nm is used. At 360 nm, however, both the cluster species as well as the monomer are photolyzed.

5. Conclusion

Extending our previous study on the OClO monomer photodissociation,[8] we investigated the photolysis of OClO clusters in a cold beam. Created under jet expansion with Ne as a carrier gas, the beam was found to contain the OClO dimer, trimer, and inhomogeneous clusters of the form $(OClO)_nNe_m$ as well as the OClO monomer. Using excitation at 360 nm, which is close to the maximum of the $\tilde{A}^2A_2 \leftarrow \tilde{X}^2B_1$ transition band in OClO, the TOF spectra revealed fast ClO photofragments from the monomer dissociation and slow OClO, O_2, Cl_2O_3, and Cl_2O_4 products having a recoil anisotropy $\beta \approx 0$, as measured for the representative OClO product. These product species agree with the previous findings of Flesch et al.[26] The broadly, almost thermally distributed translational energy observed for the slow moving fragments with $\beta \approx 0$ and the product yield (measured for OClO and O_2) following closely the cluster formation are strong indications that their formation is associated with clusters and, more specifically, that they are evaporation products of excited clusters. A reaction scheme accommodating the products is proposed which includes unimolecular, primary, and

secondary photochemical decays and bimolecular cage reactions of initially created fragments among themselves and with cluster constituents. Since the structure of the dimer $(OClO)_2$ and the important Cl_2O_3 products are not known, some of the reaction steps in this scheme should be considered tentative. In this context it is noted that preliminary ab initio calculations[26,50] have shown the feasible structures of these species to be energetically very close so that their actual structures will be difficult to determine.

With increasing concentration of the OClO monomer, the absorption spectrum in a cold Ar matrix reveals a new, unstructured, and broad absorption band at 360 nm and an additional band with similar features at around 290 nm. Anticipating this latter absorption to also occur in a cluster beam, excitation at 275 nm, where no monomer absorption exists, was carried out. Parallel to the 360 nm photolysis, the slow fragments OClO, Cl_2O_3, and Cl_2O_4 were observed but with the OClO production being about twice as efficient. Thus, by crossing the cluster beam with light of 275 nm, we selectively photolyze OClO dimers and possibly higher aggregates while at 360 nm the monomer and the dimer species are photodissociated.

Acknowledgment. Support of this work by the Schweizerischer Nationalfonds zur Förderung der wissenschaftlichen Forschung is gratefully acknowledged. We thank Dr. Gregory E. Hall and Dr. Hans U. Suter for valuable discussions, Heiner A. Scheld for technical assistance, and Dr. Robert T. Carter for critically reading the manuscript.

References and Notes

(1) Butler, J. D. *Air Pollution Chemistry*; Academic Press: London, 1979.
(2) Molina, L. T.; Molina, M. J. *J. Phys. Chem.* **1987**, *91*, 433.
(3) Sanders, R. W.; Solomon, S.; Smith, J. P.; Perlinski, L.; Miller, H. L.; Mount, G. H.; Keys, J. G.; Schmeltekopf, A. L. *J. Geophys. Res.* **1993**, *98*, 7219 and references therein.
(4) Vaida, V.; Simon, J. D. *Science* **1995**, *268*, 1443.
(5) Brown, L. A.; Vaida, V.; Hanson, D. R.; Graham, J. D.; Roberts, J. T. *J. Phys. Chem.* **1996**, *100*, 3121.
(6) Davis, H. F.; Lee, Y. T. *J. Phys. Chem.* **1992**, *96*, 5681.
(7) Davis, H. F.; Lee, Y. T. *J. Chem. Phys.* **1996**, *105*, 8142.
(8) Furlan, A.; Scheld, H.; Huber, J. R. *J. Chem. Phys.* **1997**, *106*, 6538.
(9) Vaida, V.; Solomon, S.; Richard, E. C.; Rühl, E.; Jefferson, A. *Nature* **1989**, *342*, 405.
(10) Vaida, V.; Richard, E. C.; Jefferson, A.; Cooper, L. A.; Flesch, R.; Rühl, E. *Ber. Bunsen-Ges. Phys. Chem.* **1992**, *96*, 391.
(11) Bishenden, E.; Donaldson, D. J. *J. Chem. Phys.* **1994**, *101*, 9565.
(12) Baumert, T.; Herek, J. L.; Zewail, A. H. *J. Chem. Phys.* **1993**, *99*, 4430.
(13) Delmdahl, R. F.; Baumgärtel, S.; Gericke, K.-H. *J. Chem. Phys.* **1996**, *104*, 2883.
(14) Michielsen, S.; Merer, A. J.; Rice, S. A.; Freed, F. A.; Hamada, Y. J. *J. Chem. Phys.* **1981**, *74*, 3089.
(15) McDonald, D. A.; Innes, K. K. *Chem. Phys. Lett.* **1987**, *59*, 562.
(16) Richard, E. C.; Vaida, V. *J. Chem. Phys.* **1991**, *94*, 153.
(17) Richard, E. C.; Vaida, V. *J. Chem.Phys.* **1991**, *94*, 163.
(18) Arkell, A.; Schwager, I. *J. Am. Chem. Soc.* **1967**, *89*, 5999.
(19) Adrian, F. J.; Bohandy, J.; Kim, B. F. *J. Chem. Phys.* **1986**, *85*, 2692.
(20) Johnsson, K.; Engdahl, A.; Ouis, P.; Nelander, B. *J. Mol. Chem.* **1993**, *293*, 137.
(21) Müller, H. S. P.; Willner, H. *J. Phys. Chem.* **1993**, *97*, 10589.
(22) Pursell, C. J.; Conyers, J.; Denison, C. *J. Phys. Chem.* **1996**, *100*, 15450.
(23) Chang, Y. J.; Simon, J. D. *J. Phys. Chem.* **1996**, *100*, 6406.
(24) Dunn, R. C.; Anderson, J.; Foote, C. S.; Simon, J. D. *J. Am. Chem. Soc.* **1993**, *115*, 5307.
(25) Graham, J. D.; Roberts, J. T.; Anderson, L. D.; Grassian, V. H. *J. Phys. Chem.* **1996**, *100*, 19551.
(26) Flesch, R.; Wassermann, B.; Rothmund, B.; Ruehl, E. *J. Phys. Chem.* **1994**, *98*, 6263.
(27) Busch, G. E.; Mahoney, R. T.; Morse, R. I.; Wilson, K. R. *J. Chem. Phys.* **1969**, *51*, 449.
(28) Wodtke, A. M.; Lee, Y. T. In *Molecular Photodissociation Dynamics*; Ashfold, M. N. R., Baggott, J. E., Eds.; Royal Society of Chemistry: Letchworth, U.K., 1987; p 31.
(29) Ashfold, M. N. R.; Lambert, I. R.; Mordaunt, D. H.; Morley, G. P.; Western, C. M. *J. Phys. Chem.* **1992**, *96*, 2938.
(30) Felder, P. *Chimia* **1994**, *48:3*, 43.
(31) Felder, P. *Chem. Phys.* **1990**, *143*, 141.
(32) Derby, R. I.; Hutchinson, W. S. *Inorg. Synth.* **1953**, *4*, 152.
(33) Thelen, M.-A.; Felder, P.; Huber, J. R. *Chem. Phys. Lett.* **1993**, *213*, 275.
(34) Felder, P. *Chem. Phys.* **1991**, *155*, 435.
(35) Frey, J. G.; Felder, P. *Mol. Phys.* **1992**, *75*, 1419.
(36) Sparks, R. K.; Shobatake, K.; Carlson, L. R.; Lee, Y. T. *Chem. Phys.* **1981**, *75*, 3838.
(37) Kades, E.; Rösslein, M.; Huber, J. R. *J. Phys. Chem.* **1994**, *98*, 13556.
(38) Bergmann, K.; Huber, J. R. *J. Phys. Chem. A* **1997**, *101*, 259.
(39) Zabel, F. *Ber. Bunsen-Ges. Phys. Chem.* **1991**, *95*, 893.
(40) Lopez, M. J.; Siere, J. E. *J. Phys. Chem.* **1990**, *94*, 3860.
(41) Cox, R. A.; Hayman, G. D. *Nature* **1988**, *332*, 796.
(42) Christe, K. O.; Schack, C. J.; Curtis, E. C. *Inorg. Chem.* **1971**, *10*, 1589.
(43) Hradil, V. P.; Suzuki, T.; Hewitt, S. A.; Houston, P. L.; Whitaker, B. J. *J. Chem. Phys.* **1993**, *99*, 4455.
(44) Jonah, C. *J. Chem. Phys.* **1971**, *55*, 1915.
(45) Yang, S.; Bersohn, R. *J. Chem. Phys.* **1974**, *61*, 4400.
(46) Baer, S.; Hippler, H.; Rahn, R.; Siefke, M.; Seitzinger, N.; Troe, J. *J. Chem. Phys.* **1991**, *95*, 6463.
(47) Rehr, A.; Jansen, M. *Inorg. Chem.* **1992**, *31*, 4740.
(48) Burkholder, J. B.; Mauldin, R. L. I.; Yokelsen, R. J.; Solomon, S.; Ravishankara, A. R. *J. Phys. Chem.* **1993**, *97*, 7597.
(49) JANAF Thermochemical Tables, *J. Phys. Chem. Ref. Data*, **1985**, *14*, Suppl. 1.
(50) Suter, H. U.; Huber, J. R. Unpublished results.